Published in final edited form as:

Nanoscale. 2017 August 17; 9(32): 11424–11428. doi:10.1039/c7nr03838k.

Ionic selectivity and filtration from fragmented dehydration in multilayer graphene nanopores

Subin Sahu[1,2,3] and **Michael Zwolak**[1,*]

[1]Center for Nanoscale Science and Technology, National Institute of Standards and Technology, Gaithersburg, MD 20899

[2]Maryland Nanocenter, University of Maryland, College Park, MD 20742

[3]Department of Physics, Oregon State University, Corvallis, OR 97331

Abstract

Selective ion transport is a hallmark of biological ion channel behavior but is a major challenge to engineer into artificial membranes. Here, we demonstrate, with all-atom molecular dynamics simulations, that bare graphene nanopores yield measurable ion selectivity that varies over one to two orders of magnitude simply by changing the pore radius and number of graphene layers. Monolayer graphene does not display dehydration-induced selectivity until the pore radius is small enough to exclude the first hydration layer from inside the pore. Bi- and tri-layer graphene, though, display such selectivity already for a pore size that barely encroaches on the first hydration layer, which is due to the more significant water loss from the second hydration layer. Measurement of selectivity and activation barriers from both first and second hydration layer barriers will help elucidate the behavior of biological ion channels. Moreover, the energy barriers responsible for selectivity – while small on the scale of hydration energies – are already relatively large, i.e., many k_BT. For separation of ions from water, therefore, one can exchange longer, larger radius pores for shorter, smaller radius pores, giving a practical method for maintaining exclusion efficiency while enhancing other properties (e.g., water throughput).

Ion transport is vital to physiological processes in the cell [1–3], where membrane ion channels control ion motion through the interplay of protein structural transitions, precisely placed dipoles and charges, and dehydration. Nanotechnologies seek to mimic and exploit the same physical mechanisms for membrane filtration and desalination. However, biological systems are complex and make use of sophisticated assembly methods, ones that remain difficult to utilize in artificial devices. Recent work, though, on two-dimensional channels in graphene laminates demonstrates ion selectivity [4] by constraining the channel height. One-dimensional channels – pores – give additional control over the confining geometry, where, for instance, recent theoretical results [5] show that experiments on sub-nanoscale, monolayer graphene pores likely display dehydration-only selectivity [6].

Using all-atom molecular dynamics (MD) simulation and theoretical arguments, we show that the most fundamental of all processes – dehydration of ions – can be reliably tuned in

*Corresponding Author: mpz@nist.gov.

bare graphene nanopores by controlling only the pore radius and number of graphene layers. This gives rise to selectivity across one to two orders of magnitude before ion currents drop to unmeasurable levels. This range of achievable selectivities is possible due to the ability to separately control the pore radius and length at the nanoscale, i.e., in the regime that influences the hydration layers via the confinement.

Figure 1 shows how the hydration layers change for mono- to trilayer graphene pores. As an ion goes from bulk into the pore, it can not bring its whole hydration layer with it, but rather some of the water molecules are blocked from entering the pore. The shedding of some of the hydration gives a free energy barrier, a simple estimate of which is,

$$\Delta F_\nu = \sum_i f_{i\nu} E_{i\nu}, \quad (1)$$

where, $f_{i\nu}$ ($E_{i\nu}$) is the fractional dehydration (energy) in the i^{th} hydration layer [7, 8]. The fractional dehydration depends on the confinement via the pore radius and length (number of graphene layers), as this reduces the volume available for water to hydrate the ion. That is,

$$f_{i\nu} = \frac{\Delta n_i}{n_i} \approx \frac{\Delta V_i}{V_i}, \quad (2)$$

with the total hydration number n_i and volume V_i of the i^{th} hydration layer in bulk and the reduction, Δn_i and ΔV_i, of those respective quantities in the pore. The quantity ΔV_i comes from pure geometric arguments –it is the volume excluded by the presence of graphene carbon atoms – and the approximation in Eq. 2 agrees well with the loss of water molecules computed from MD simulations [shown in Fig. 1(b)]. For narrow pores that split the hydration layer into two hemispherical caps, one can use the surface area available for waters to hydrate the ion, instead of volumes [5, 7, 8]. The Supplementary Information (SI) contains additional details.

For the radius r_p = 0.34 nm pore in Fig. 1(a), this simple analytic estimate predicts that there should be a small amount of dehydration in the first layer, increasing when going from mono- to bi-/tri-layer graphene. For the multilayer graphene, though, the second hydration layer is significantly reduced. However, due to the much larger hydration energy of the first layer [8], both hydration layers influence the magnitude of the ion currents and thus the selectivity. Moreover, the contribution to the dehydration free energy barrier from hydration layer i will "level off" when the length is greater than about twice its radius, i.e., when part of the hydration layer can no longer reside outside of the pore.

This is exactly what is seen from free energy computations using MD. Fig. 2(a) shows the free energy barrier for K^+ and Cl^- moving through the pore. Monolayer graphene interferes very little with the hydration for this pore radius. To the extent that this membrane dehydrates the ions, the remaining water molecule can partially compensate for this effect by

more strongly orienting their dipole moment with the ion, see the SI. When the number of layers increases, however, the energy barriers change in size and shape. For both bi- and tri-layer graphene, the dehydration is more substantial and, when accounting for the larger Cl^- hydration energy, it starts to differentiate between the two ions. That is, the relative barriers are predominantly influenced by the hydration energies of the different ions. As the confinement increases – decreasing the pore radius and increasing the pore length – more water will be lost from the hydration layers, and ions with larger hydration energies will be more effectively filtered by the pore and selected against. Fig. 2(b) shows this effect, i.e., how the dehydration and free energy barriers increase with increasing number of graphene layers.

The free energy barriers are the primary factor in determining permeation rates and ion currents. For instance, the current in the pore is related to the free energy barrier and electric field E according to [8]

$$I_\nu = e z_\nu \mu_\nu^{\text{eff}} E A_p n_\nu e^{-\Delta F_\nu / k_B T}, \quad (3)$$

where, e is the electric charge, z_ν the ion valency, μ_ν^{eff} the effective mobility in the pore, A_p is the area of the pore, n_ν the bulk ion density, k_B is Boltzmann's constant, and T is the temperature. The factors that contribute to selectivity are μ_ν^{eff} and ΔF_ν (and, to some extent, the accessible area for transport is ion dependent as it relates to hydrated ion size. This can be neglected here.). For atomically thin graphene membranes, one expects that the effective mobility is ill-defined. Even still, its contribution to selectivity should be of order 1 (for instance, the ratio of effective mobilities of K^+ and Cl^- goes from about 1 in bulk to about 1.2 in α-hemolysin [9]). We can thus estimate selectivity as

$$\frac{I_{\text{K}}}{I_{\text{Cl}}} \approx e^{(\Delta F_{\text{K}} - \Delta F_{\text{Cl}})/k_B T}. \quad (4)$$

This is, however, only an estimate: In addition to the effects just discussed, the energy landscape has some ion-dependent spatial structure (which introduces additional factors into the current), and it changes when a bias is applied. For instance, the applied field orients the water dipoles, which can subsequently chaperone ions across the pore [5]. Eq. 4, though, gives the expected scale for selectivity.

Using nonequilibrium MD, we directly compute $I_{\text{K}}/I_{\text{Cl}}$ where possible and use Eq. 4 otherwise. Fig. 3 shows the selectivity for pores of radii ranging from 0.21 nm to 0.79 nm in mono-, bi-, and tri-layer graphene. Just as the above theoretical arguments and free energy simulations indicate, the relative current of K^+ increases compared to Cl^- as the pore radius approaches the hydration. The magnitude of this selectivity depends on the pore radius as well as the number of graphene layers. We note that the pores are electrically neutral and contain no dipoles. Hence, the selectivity is due to differences in their hydration energies of

the ions. All ion types will thus display mutual selectivity. We also note that chemical functionalization of the pore and of the graphene can modify energy barriers, especially when, e.g., the chemical groups are strongly polar or charged under some ionic conditions. When this occurs, the sign of the charge matters, and anions, for instance, may be excluded from the pore. Thus, the selectivity between cations and anions due to a charged pore will be stronger and observable for larger pores, as seen in Ref. 10. However, the effect we discuss will never-the-less be present between cations, where Eqs. 1 and 2 can estimate the selectivity.

The selectivity that is measurable experimentally will be limited by the minimum resolvable current. The Cl^- current is about 5 pA for the 0.34 nm trilayer pore (see Table S1 in the SI). Currents as low as 1 pA are measurable in experiments [11]; thus a several fold change in selectivity should be detectable as the pore size and length vary. This will enable the experimental extraction of dehydration energy barriers (via the temperature dependence of the current) versus the size (length and radius) of this artificial “selectivity filter”.

Moreover, this provides a method to control selectivity beyond just changing the pore radius so that, e.g., other aspects of the device can be controlled for. According to Ref. 12, the water flow rate only decreases by about 20 % when going from mono- to bi- layer graphene when the pore size is kept constant, and there is no additional inter-layer spacing. Increasing the number of layers to increase selectivity (or ion exclusion overall) will not significantly reduce water flow for applications such as desalination. Moreover, for a given selectivity or ion exclusion, one can use a larger pore with more layers, increasing the overall water throughput (as the area available for transport is larger) and membrane stability.

These results indicate that to achieve a given selectivity, one can exchange a $r_p = 0.21$ nm monolayer pore with a trilayer pore of a larger radius ($r_p = 0.34$ nm). These pore sizes are both clearly small, but this indicates that, *when dealing with nanostructures*, there is flexibility on how to create the desired ion exclusion. Pore sizes are controllable with individual pores fabricated with transmission electron microscopes [13–15] and techniques are under development to fabricate large scale membranes with precise control [6, 16]. Moreover, we examine only pores with high symmetry. Varying the aspect ratio and the shape of the pore can further tune the conductance and the ion selectivity provided the lateral dimensions of the pore are on the scale of hydration. In any case, layering gives an additional, discrete “knob” to tune selectivity and exclusion.

Ion transport through sub-nanometer channels, where dehydration is inevitable, is a key process in biology. Ion transport at this scale is also increasingly important in applications, such as nanopore sequencing (both ionic [17–19] and electronic [20–22]), desalination [23] and filtration [24]. Graphene membranes and laminates, as well as other atomically thick membranes, are playing a central role, where selective ion transport and ion exclusion is desired [4–6, 10, 25–27]. Moreover, fundamental studies demonstrate the possibilities of seeing ionic analogs of electric phenomena, such as quantized ionic conductance [7, 8] and ionic Coulomb blockade [28, 29].

Our results form the basis for engineering and understanding selectivity and exclusion with multilayer graphene pores, where both the radial and longitudinal lengths can be controlled at the sub-nanoscale level. This is a feat not easily achievable with other approaches, e.g., solid state [7, 8] or carbon nanotubes [30–32] (despite some success in making ultra-thin solid state pores[33]). Moreover, examining pores with intermediate pore radii (but "non-circular") may show that there is a notion of *quantized ionic selectivity*, that for, e.g., trilayer graphene, as the pore radius is reduced, the second hydration layer first gives rise to selectivity, and then the first layer (see the SI for an extended discussion). Channel/pore geometry gives a range of possibilities for designing selective pores and experimentally delineating the role of dehydration (to, e.g., understand more complex biological ion channels). Chemical functionalization [34] and other factors give further possibilities for modifying and engineering selective behavior.

Methods

We perform all-atom molecular dynamics (MD) simulations using NAMD2 [35] with the time step of 2 fs and periodic boundary condition in all directions. The water model is rigid TIP3P [36] from the CHARMM27 force field. Bi- and tri-layer graphene has AB and ABA stacking, respectively. The real-time current comes from applying a 1 V potential across the simulation cell and counting the ion crossing events. The free energies are from equilibrium MD simulations using the adaptive biasing force (ABF) method [37, 38]. The SI contains additional details regarding methodology. Movie S1, Movie S2, and Movie S3 show a K^+ ion translocating through mono-, bi-, and tri-layer graphene pores, respectively.

Supplementary Material

Refer to Web version on PubMed Central for supplementary material.

Acknowledgments

We thank J. Elenewski and M. Di Ventra for helpful comments. S. Sahu acknowledges support under the Cooperative Research Agreement between the University of Maryland and the National Institute of Standards and Technology Center for Nanoscale Science and Technology, Award 70NANB14H209, through the University of Maryland.

References

1. Hille, B. Ion channels of excitable membranes. Vol. 507. Sinauer Sunderland; MA: 2001.
2. Bagal SK, Brown AD, Cox PJ, Omoto K, Owen RM, Pryde DC, Sidders B, Skerratt SE, Stevens EB, Storer RI, Swain NA. J Med Chem. 2012; 56:593. [PubMed: 23121096]
3. Rasband MN. Nature Education. 2010; 3:41.
4. Abraham J, Vasu KS, Williams CD, Gopinadhan K, Su Y, Cherian CT, Dix J, Prestat E, Haigh SJ, Grigorieva IV, Carbone P, Geim AK, Nair RR. Nat Nanotechnol. 2017; 12:546. [PubMed: 28369049]
5. Sahu S, Di Ventra M, Zwolak M. Nano Lett. 2017; 17:4719. arXiv:1605.03134 (2016). [PubMed: 28678508]
6. O'Hern SC, Boutilier MSH, Idrobo JC, Song Y, Kong J, Laoui T, Atieh M, Karnik R. Nano Lett. 2014; 14:1234. [PubMed: 24490698]
7. Zwolak M, Lagerqvist J, Di Ventra M. Phys Rev Lett. 2009; 103:128102. [PubMed: 19792463]
8. Zwolak M, Wilson J, Di Ventra M. J Phys: Condens Matter. 2010; 22:454126. [PubMed: 21152075]

9. Bhattacharya S, Muzard J, Payet L, Mathé J, Bockelmann U, Aksimentiev A, Viasnoff V. J Phys Chem C. 2011; 115:4255.
10. Rollings RC, Kuan AT, Golovchenko JA. Nat Commun. 2016; 7:11408. [PubMed: 27102837]
11. Balijepalli A, Ettedgui J, Cornio AT, Robertson JW, Cheung KP, Kasianowicz JJ, Vaz C. ACS Nano. 2014; 8:1547. [PubMed: 24397836]
12. Cohen-Tanugi D, Lin LC, Grossman JC. Nano Lett. 2016; 16:1027. [PubMed: 26806020]
13. Garaj S, Hubbard W, Reina A, Kong J, Branton D, Golovchenko J. Nature. 2010; 467:190. [PubMed: 20720538]
14. Schneider GF, Kowalczyk SW, Calado VE, Pandraud G, Zandbergen HW, Vandersypen LM, Dekker C. Nano Lett. 2010; 10:3163. [PubMed: 20608744]
15. Merchant CA, Healy K, Wanunu M, Ray V, Peterman N, Bartel J, Fischbein MD, Venta K, Luo Z, Johnson AC, Drndić M. Nano Lett. 2010; 10:2915. [PubMed: 20698604]
16. Jain T, Rasera BC, Guerrero RJS, Boutilier MS, O'Hern SC, Idrobo JC, Karnik R. Nat Nanotechnol. 2015; 10:1053. [PubMed: 26436566]
17. Kasianowicz JJ, Brandin E, Branton D, Deamer DW. Proc Natl Acad Sci U S A. 1996; 93:13770. [PubMed: 8943010]
18. Clarke J, Wu HC, Jayasinghe L, Patel A, Reid S, Bayley H. Nat Nanotechnol. 2009; 4:265. [PubMed: 19350039]
19. Sathe C, Zou X, Leburton JP, Schulten K. ACS Nano. 2011; 5:8842. [PubMed: 21981556]
20. Zwolak M, Di Ventra M. Nano Lett. 2005; 5:421. [PubMed: 15755087]
21. Lagerqvist J, Zwolak M, DiVentra M. Nano Lett. 2006; 6:779. [PubMed: 16608283]
22. Zwolak M, Di Ventra M. Rev Mod Phys. 2008; 80:141.
23. Lee KP, Arnot TC, Mattia D. J Membr Sci. 2011; 370:1.
24. Karan S, Jiang Z, Livingston AG. Science. 2015; 348:1347. [PubMed: 26089512]
25. Walker MI, Ubych K, Saraswat V, Chalklen EA, Braeuninger-Weimer P, Caneva S, Weatherup RS, Hofmann S, Keyser UF. ACS Nano. 2017; 11:1340. [PubMed: 28157333]
26. Surwade SP, Smirnov SN, Vlassiouk IV, Unocic RR, Veith GM, Dai S, Mahurin SM. Nat Nanotechnol. 2015; 10:459. [PubMed: 25799521]
27. Joshi R, Carbone P, Wang F, Kravets V, Su Y, Grigorieva I, Wu H, Geim A, Nair R. Science. 2014; 343:752. [PubMed: 24531966]
28. Krems M, Di Ventra M. J Phys: Condens Matter. 2013; 25:065101. [PubMed: 23307655]
29. Feng J, Liu K, Graf M, Dumcenco D, Kis A, Di Ventra M, Radenovic A. Nat Mater. 2016; 15:850. [PubMed: 27019385]
30. Song C, Corry B. J Phys Chem B. 2009; 113:7642. [PubMed: 19419185]
31. Richards LA, Schäfer AI, Richards BS, Corry B. Small. 2012; 8:1701. [PubMed: 22434668]
32. Richards LA, Schäfer AI, Richards BS, Corry B. Phys Chem Chem Phys. 2012; 14:11633. [PubMed: 22821005]
33. Rodríguez-Manzo JA, Puster M, Nicoläi A, Meunier V, Drndić M. ACS Nano. 2015; 9:6555. [PubMed: 26035079]
34. Sint K, Wang B, Král P. J Am Chem Soc. 2008; 130:16448. [PubMed: 19554715]
35. Phillips JC, Braun R, Wang W, Gumbart J, Tajkhorshid E, Villa E, Chipot C, Skeel RD, Kale L, Schulten K. J Comput Chem. 2005; 26:1781. [PubMed: 16222654]
36. Jorgensen WL, Chandrasekhar J, Madura JD, Impey RW, Klein ML. J Chem Phys. 1983; 79:926.
37. Darve E, Rodríguez-Gómez D, Pohorille A. J Chem Phys. 2008; 128:144120. [PubMed: 18412436]
38. Hénin J, Chipot C. J Chem Phys. 2004; 121:2904. [PubMed: 15291601]

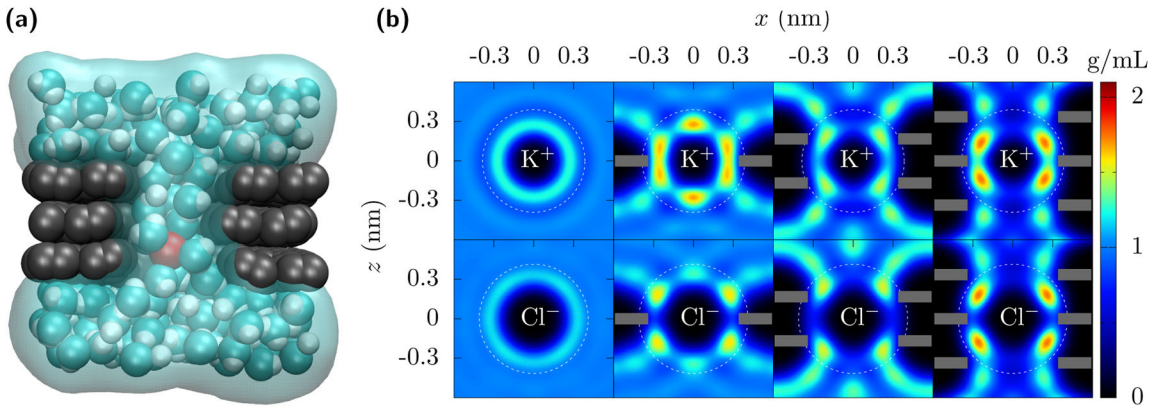

FIG. 1. Dehydration of ions going through multilayer graphene pores

(a) A nanopore through trilayer graphene. As K^+ (red) translocates through the pore, it retains only part of its hydration. In this case, the pore radius is $r_p = 0.34$ nm and the first hydration layer is essentially complete. The second hydration layer, though, is significantly diminished due to the carbon of the graphene (gray) preventing the water molecules (cyan and white) from fluctuating about 0.5 nm away from the ion, except along the pore axis. **(b)** Water density quantified by its oxygen location around K^+ and Cl^- ions fixed in bulk and in the center of mono-, bi-, and tri-layer graphene (shown as grey bars) pores with radius $r_p = 0.34$ nm. The white dotted circles demarcate the first and the second hydration layers. The first hydration layers remain but acquire some additional structure. The second hydration layer is greatly reduced (see Fig. 2, and Fig. S2 and Table S2 in the SI). For this pore size, the free energy barrier due to the second layer dehydration significantly contributes to the ion currents and selectivity. The bi- and tri-layer graphene are AB and ABA stacked, respectively, but similar results occur for perfectly aligned multilayer graphene.

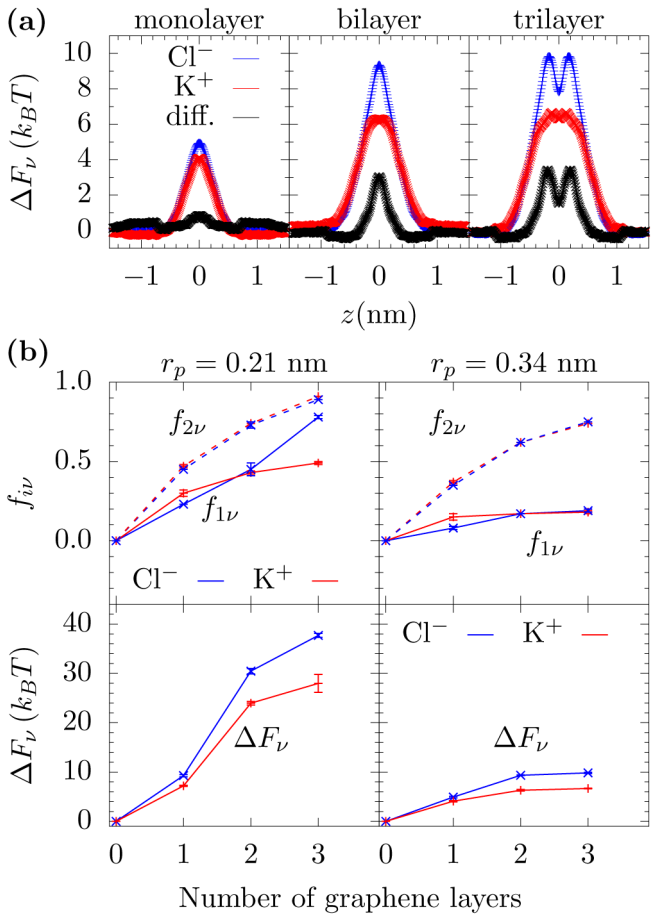

FIG. 2. Free energy barriers and dehydration

(a) Free energy barrier versus K^+ and Cl^- location, z, on the pore axis as they cross mono-, bi-, and tri-layer graphene pores with radius 0.34 nm. As the number of layers increases, the energy barrier becomes more substantial and a difference between the two ion types appears. **(b)** Fractional dehydration in the first and second layer ($f_{1\nu}$ and $f_{2\nu}$) for K^+ and Cl^-, where the ion is at the position of its free energy maximum in the pore. When the pore radius is less than the first hydration layer radius (about 0.3 nm), then both the first and second hydration layers lose a substantial amount of their water molecules (upper left panel). However, with just a slightly larger pore radius, r_p = 0.34 nm, the first hydration layer retains most of its water but the second layer still loses a significant number of water molecules (upper right panel). The free energy barriers (lower panels) will increase with the number of graphene layers, as a "short pore" interferes less with the hydration than the longer pores. However, while dehydration is the mechanism by which selectivity occurs, water loss is not the sole predictor of selectivity. As Eq. 1 shows, one also needs the hydration layer energies. The Cl^- ion has a larger hydration energy and, thus, even for the same $f_{i\nu}$, Cl^- will be selected against. Error bars are ±1 standard error from five parallel simulations.

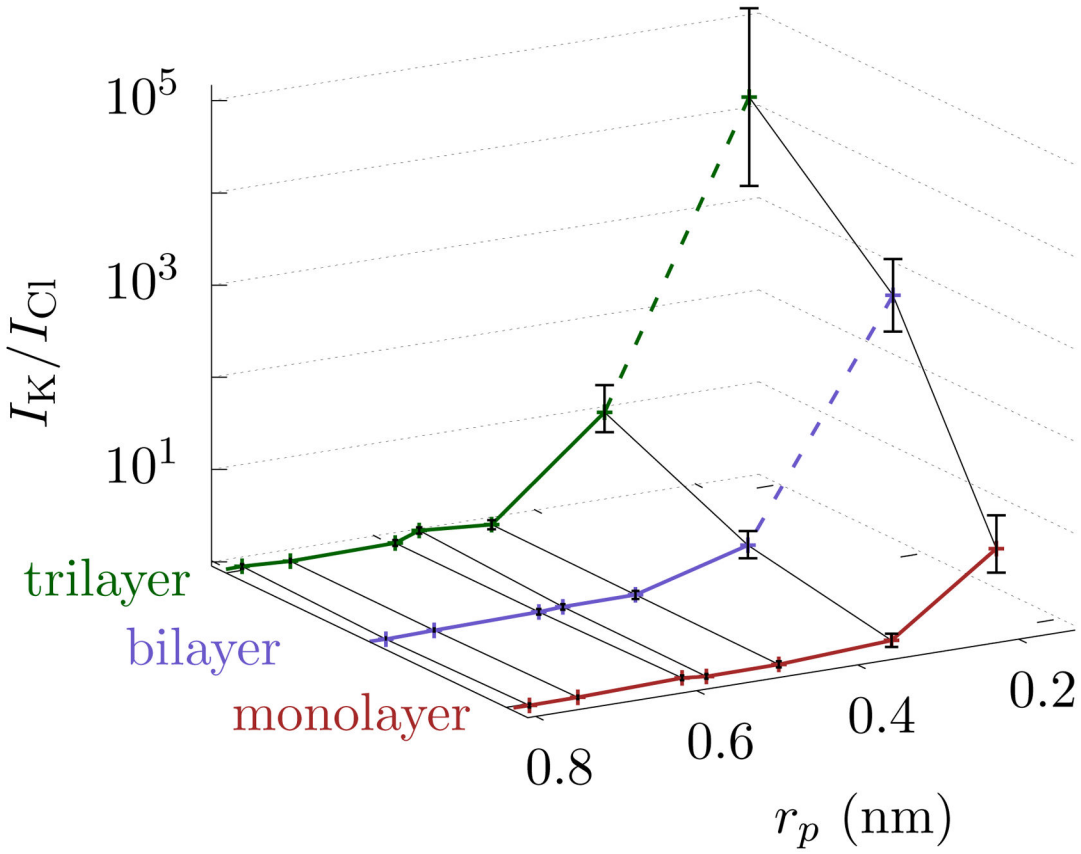

FIG. 3. Selectivity of graphene pores

The selectivity, I_K/I_{Cl}, is at an applied bias of 1 V, although the permeation rates should follow similar trends. Selectivity increases as pore radius decreases and when the number of layers increases. Trilayer graphene with r_p = 0.34 nm gives a similar selectivity as monolayer graphene with r_p = 0.21 nm. Moreover, if only ion filtration is of interest, then these two pore sizes can be exchanged. For bi- and tri-layer graphene, we use Eq. 4 for r_p = 0.21 nm, as the currents are too small to reliably determine computationally. Those points have a dashed line connecting them to the remaining plot. The error bars are ± 1 block standard error (BSE).